BIOCHEMISTRY
including biophysical chemistry & molecular biology

Article

pubs.acs.org/biochemistry

The Structure of Allophanate Hydrolase from *Granulibacter bethesdensis* Provides Insights into Substrate Specificity in the Amidase Signature Family

Yi Lin and Martin St. Maurice*

Department of Biological Sciences, Marquette University, Milwaukee, Wisconsin 53201, United States

Supporting Information

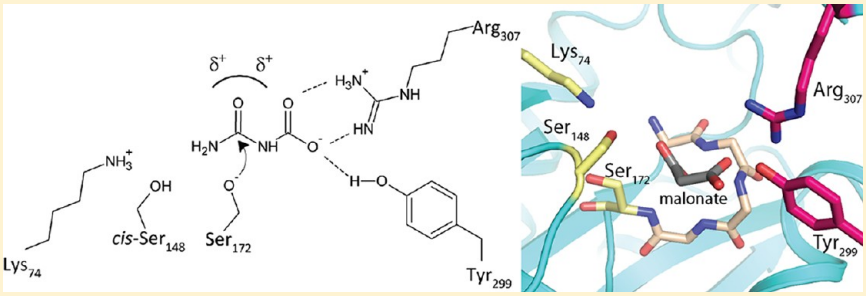

ABSTRACT: Allophanate hydrolase (AH) catalyzes the hydrolysis of allophanate, an intermediate in atrazine degradation and urea catabolism pathways, to NH_3 and CO_2. AH belongs to the amidase signature family, which is characterized by a conserved block of 130 amino acids rich in Gly and Ser and a Ser-*cis*-Ser-Lys catalytic triad. In this study, the first structures of AH from *Granulibacter bethesdensis* were determined, with and without the substrate analogue malonate, to 2.2 and 2.8 Å, respectively. The structures confirm the identity of the catalytic triad residues and reveal an altered dimerization interface that is not conserved in the amidase signature family. The structures also provide insights into previously unrecognized substrate specificity determinants in AH. Two residues, Tyr_{299} and Arg_{307}, are within hydrogen bonding distance of a carboxylate moiety of malonate. Both Tyr_{299} and Arg_{307} were mutated, and the resulting modified enzymes revealed >3 order of magnitude reductions in both catalytic efficiency and substrate stringency. It is proposed that Tyr_{299} and Arg_{307} serve to anchor and orient the substrate for attack by the catalytic nucleophile, Ser_{172}. The structure further suggests the presence of a unique C-terminal domain in AH. While this domain is conserved, it does not contribute to catalysis or to the structural integrity of the core domain, suggesting that it may play a role in mediating transient and specific interactions with the urea carboxylase component of urea amidolyase. Analysis of the AH active site architecture offers new insights into common determinants of catalysis and specificity among divergent members of the amidase signature family.

Allophanate hydrolase (AH, EC 3.5.1.54) catalyzes the hydrolysis of allophanate to ammonia and carbon dioxide (Scheme 1). It is a member of the amidase signature (AS) family,

Scheme 1

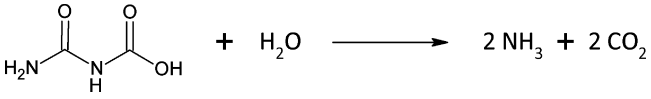

characterized by a highly conserved stretch of up to 130 amino acids rich in serine and glycine.[1,2] The AS family is currently known to include more than 200 different enzymes in organisms ranging from bacteria to plants and mammals.[3] These enzymes participate in diverse biological activities, including the catabolism of neuromodulatory fatty acids in mammals by fatty acid amide hydrolase,[4] formation of Gln-tRNA^{Gln} by GatCAB in a subset of bacteria,[5] formation of the plant development regulator, indole-3-acetic acid, by nitrile hydratase,[6] and the hydrolysis of malonamate by malonamidase in the transport of nitrogen from the bacteroid to the plant during nitrogen fixation.[7] In addition, AS family enzymes have been implicated in a variety of industrial applications, such as the degradation of nylon polymers[8,9] and the amidation of synthetic peptides.[10] AS family enzymes utilize a conserved Ser-*cis*-Ser-Lys triad to catalyze amide bond hydrolysis, where the underlined serine residue serves as the catalytic nucleophile.[11] Nucleophilic attack by serine results in a covalent tetrahedral intermediate that is stabilized by an oxyanion hole. After ammonia had been displaced, the covalent intermediate is hydrolyzed to release the product. Although the catalytic triad is conserved, AS family enzymes exhibit a wide variation in residues that contribute to substrate specificity. Given the broad cross section of substrates upon which AS family enzymes act, this family serves as an

Received: September 12, 2012
Revised: December 15, 2012
Published: January 2, 2013

intriguing paradigm for relating molecular architecture to substrate specificity.

AH was first characterized as one domain of the multifunctional fungal enzyme urea amidolyase. Urea amidolyase is a biotin-dependent enzyme comprised of two separate enzymatic activities, urea carboxylase and AH, that hydrolyze urea to ammonia and carbon dioxide in a two-step process. A carboxyl group is added to urea by urea carboxylase, forming allophanate, which is subsequently hydrolyzed into ammonia and carbon dioxide by AH. Urea amidolyase is the terminal enzyme of urea degradation and arginine catabolism.[12,13] It is a virulence factor in *Candida albicans*, an opportunistic pathogen that can evade the human immune system and cause lethal infections in immunocompromised patients. The urea carboxylase component of *Kluyveromyces lactis* urea amidolyase was recently crystallized and characterized.[14] However, the structure of the AH domain remains undefined.

Unlike urea amidolyase enzymes in fungi, urea carboxylase and AH exist as separate subunits in bacteria.[15,16] It is not clear whether and to what degree these subunits physically interact to affect bacterial urea amidolyase activity. In addition, Shapir et al.[17] have determined that AH from *Pseudomonas* sp. strain ADP-1 is involved in cyanuric acid metabolism and that this enzyme has no association with urea carboxylase. In this pathway, AH serves as the terminal enzyme in *s*-triazine ring catabolism and serves an important role in the biodegradation of herbicides such as atrazine. Phylogenetic analysis has revealed that AH is broadly distributed in bacteria, where it functions in the metabolism of both cyanuric acid and urea.[18]

Here we report the first crystal structures of AH, both with and without a bound substrate analogue, malonate, in the active site. The structure of AH from the bacterium *Granulibacter bethesdensis* confirms the location of the Ser-*cis*-Ser-Lys catalytic triad conserved throughout the AS family. Comparison of the AH structure to those from other AS family enzymes offers insights into substrate specificity determinants in AH. Two amino acids, Tyr_{299} and Arg_{307}, are conserved in AH and are within hydrogen bonding distance of the substrate analogue. Steady-state kinetic analysis of Tyr_{299} and Arg_{307} site-directed mutants reveals that the ratio of the specificity constant (k_{cat}/K_m) for allophanate compared to biuret decreases ~200-fold for Y299F and that the R307A and R307M mutants are nearly inactive. These results suggest a role for these residues in providing substrate and intermediate stabilization in AH. Finally, the structure suggests the presence of an additional C-terminal domain that is unique to AH and that may act as a functional linker between urea carboxylase and AH.

MATERIALS AND METHODS

Materials. IPTG, NADH, and kanamycin were purchased from Research Products International Corp. (Mount Prospect, IL). Ni^{2+}-Profinity IMAC resin was obtained from Bio-Rad (Hercules, CA). Q-Sepharose ion-exchange resin was obtained from Amersham Biosciences, GE Healthcare (Pittsburgh, PA). All other materials were obtained from Sigma-Aldrich. Potassium allophanate was prepared by hydrolyzing ethyl allophanate (Acros Organics, Fisher Scientific, Pittsburgh, PA) as described previously.[19]

Construction of an Expression Vector for His-Tagged Allophanate Hydrolase. Genomic DNA from *G. bethesdensis* (strain ATCC BAA-1260/CGDNIH1) was obtained from American Type Culture Collection (Manassas, VA). The allophanate hydrolase gene (GenBank entry ABI62642.1) was amplified by polymerase chain reaction (PCR) using the primers 5′-GAA GCT GCA GAT GAC GCT GAG CAT G-3′ and 5′-CAG ACT CGA GCT TAC TGC GCC AAA TA-3′. Primers were synthesized by Integrated DNA Technologies (Coralville, IA). The PCR-amplified fragment was digested with PstI and XhoI and ligated into the PstI- and XhoI-digested pET28a-$(His)_8$-TEV vector, downstream of the T7 promoter, N-terminal $(His)_8$ tag, and rTEV protease recognition sequence.[20] The Tyr_{299} and Arg_{307} single and double mutations were generated for this study by QuikChange site-directed mutagenesis (Stratagene, La Jolla, CA) using Pfu Turbo polymerase. The complete sequence of all cloned and mutagenized genes was verified by Functional Biosciences (Madison, WI).

Overexpression and Purification of Protein. *Escherichia coli* HMS174(DE3) cells were transformed with the pET28a-$(His)_8$-TEV plasmid encoding wild-type or mutagenized *Gb*AH and were grown in LB medium containing 25 μg/mL kanamycin. LB medium (1 L) was inoculated with a single colony transformant and incubated overnight at 37 °C. The overnight culture was used to inoculate 12 L of LB medium that was grown at 37 °C to an OD_{600} of 0.8. The cultures were chilled in an ice/water bath prior to induction with IPTG to a final concentration of 1 mM. The cultures were transferred to a 16 °C shaking incubator for 24 h prior to cell harvesting.

Both wild-type and mutant *Gb*AH were purified using Ni^{2+}-affinity and ion-exchange chromatography. The harvested cells were disrupted by sonication in buffer containing 50 mM HEPES (pH 8.0), 300 mM NaCl, and 0.1 mM EGTA and centrifuged at 12000 rpm and 4 °C prior to being loaded onto a column containing 10 mL of Ni^{2+}-Profinity IMAC resin. The column was washed using buffer containing 20 mM imidazole, and the protein was eluted from the column using a gradient from 20 to 300 mM imidazole, with *Gb*AH eluting between 100 and 250 mM. The purified protein was subsequently pooled and dialyzed overnight at 4 °C against buffer containing 20 mM HEPES (pH 8.0), 50 mM NaCl, 1 mM EGTA, and 2 mM DTT prior to being loaded onto a 10 mL Q-Sepharose ion-exchange column. The column was washed using buffer containing 50 mM NaCl, and the protein was eluted using a gradient from 100 to 750 mM NaCl. The purified protein fractions were pooled, concentrated to 17 mg/mL, dialyzed overnight at 4 °C against storage buffer containing 10 mM HEPES (pH 8.0), 50 mM NaCl, and 1 mM DTT, and drop-frozen in liquid nitrogen for storage at −80 °C. The protein concentration was determined spectrophotometrically using the calculated molar extinction coefficient for *G. bethesdensis* AH of 61810 M^{-1} cm^{-1} at 280 nm.[21] Typical yields were ~10 mg/L. The purity and subunit molecular mass were estimated by sodium dodecyl sulfate−polyacrylamide gel electrophoresis (SDS−PAGE). The purity was >99%, and the molecular mass was determined to be ~65 kDa. Analytical gel filtration chromatography was performed on a Superose 6 HR 10/30 column (GE Healthcare) in buffer containing 20 mM HEPES (pH 7.5), 150 mM NaCl, and 1 mM DTT.

Protein Crystallization. Crystals of *Gb*AH, both with and without malonate, were grown at room temperature by the hanging-drop vapor diffusion method. Crystals of *Gb*AH with malonate were obtained from a well solution of 100 mM PIPES (pH 6.5) and 1.04 M sodium malonate. The crystals of apo *Gb*AH were obtained from a well solution of 100 mM HEPES (pH 7.5), 24% PEG 4K, and 50 mM $MgCl_2$. In both cases, the protein solution (4 mg/mL) and reservoir solution were mixed in a 1:1 ratio, yielding a final volume of 5 μL. The initial *Gb*AH crystals grew spontaneously from a well solution of 100 mM

PIPES (pH 6.5) and 1.04 M sodium malonate after 2 months. Subsequently, all drops were microseeded with pulverized *Gb*AH crystals ~24 h after mixing. The resulting diamond-shaped *Gb*AH crystals grew within 5−7 days of seeding. After 10−15 days, the crystals of *Gb*AH with malonate were transferred to a cryoprotectant solution consisting of 6 M sodium malonate and 100 mM PIPES (pH 6.5). The crystals of apo *Gb*AH were transferred to a cryoprotectant solution consisting of 100 mM HEPES (pH 7.5), 35% PEG 4K, and 50 mM $MgCl_2$. All crystals were flash-cooled in a nitrogen gas stream at 100 K.

The crystals belonged to space group $P6_1$, with two subunits in the asymmetric unit and the following unit cell parameters: a = 78 Å, b = 78 Å, c = 395 Å, $\alpha = \beta = 90°$, and $\gamma = 120°$.

Data Collection, Structure Determination, and Refinement. X-ray diffraction data were collected at Sector 21 (LS-CAT) of the Advanced Photon Source (APS, Chicago, IL). The diffraction data for *Gb*AH with malonate were collected using beamline 21-ID-D with a MAR 300 CCD detector at a wavelength of 1.033 Å. The diffraction data for apo *Gb*AH were collected using beamline 21-ID-F with a MAR 225 CCD detector at a wavelength of 1.033 Å. Diffraction images were processed with HKL2000.[22] The structure of *Gb*AH with malonate was determined by molecular replacement using a putative amidase protein [Protein Data Bank (PDB) entry 2DC0] as the search model using AutoMR[23] from the Phenix software suite. The apo *Gb*AH structure was determined by molecular replacement using *Gb*AH with malonate as the search model with AutoMR. The initial models were subsequently built with AutoBuild,[24] extended by several rounds of manual model building with COOT,[25] and refined with Phenix.Refine.[26] Water molecules were added to the model in COOT with subsequent manual verification. Data collection and processing statistics are summarized in Table 1. The long unit cell axis of 395 Å resulted in some overlapping reflections. This was particularly problematic for data collected on the MAR 225 CCD detector on LS-CAT-21-ID-F. Consequently, the values for R_{merge} and some refinement statistics are slightly elevated but still fall well within the acceptable range.

Enzyme Assays. The activity of wild-type *Gb*AH and Tyr_{299} mutants with allophanate was assayed using a glutamate-dehydrogenase coupled assay at 340 nm[27] in 50 mM HEPES (pH 7.4), containing 50 mM NaCl and 1 mM EGTA in the presence of 10 mM allophanate, 40 units of glutamate-dehydrogenase (GDH), 20 mM α-ketoglutarate, and 0.5 mM NADH. The activity of *Gb*AH with substrate analogues and the activity of the *Gb*AH Arg_{307} mutant with allophanate were assayed using a fixed-time phenol-hypochlorite assay in 50 mM HEPES (pH 7.4), 150 mM NaCl, and 1 mM DTT.[28] A background rate was observed in all GDH-coupled reactions, but it was subtracted from the AH-catalyzed rate. The reaction with substrate analogues was slow and in some cases was monitored for up to 10 h to estimate rate constants. Despite the slow reaction rates, enzyme-catalyzed reactions (typically 1000 min^{-1}) could easily be measured over the very slow background rate of spontaneous hydrolysis (~20 min^{-1}). One unit of enzyme is defined as the amount of enzyme required to hydrolyze 1 mol of substrate/min at 25 °C.

Enzyme kinetic constants were estimated by nonlinear curve fitting using GraphPad Prism version 3.02 (GraphPad Software Inc., San Diego, CA). The apparent K_m and k_{cat} values were determined by fitting to the Michaelis−Menten equation for single-enzyme systems.

Table 1. Data Collection and Refinement Statistics[a]

	*Gb*AH with sodium malonate	apo *Gb*AH
PDB entry	4GYS	4GYR
space group	$P6_1$	$P6_1$
cell dimensions		
a, b, c (Å)	78, 78, 395	78, 78, 398
α, β, γ (deg)	90, 90, 120	90, 90, 120
resolution range (Å)	50−2.2 (2.26−2.20)	50−2.8 (2.87−2.80)
redundancy	9.2 (6.6)	9.0 (4.6)
completeness (%)	97.2 (96.2)	99.9 (100)
R_{merge} (%)	11.5 (33.2)	11.4 (17.1)
average I/σ	21.2 (4.9)	20.8 (18.1)
R_{work}	0.174 (0.218)	0.256 (0.296)
R_{free}	0.202 (0.275)	0.307 (0.363)
no. of reflections	66210	33600
no. of atoms	7294	6930
protein	6840	6814
others	28	0
water	426	116
Wilson B factor	31.5	40.3
average B factor (Å)		
protein	32.4	40.0
ligand	36.3	–
solvent	35.7	35.7
Ramachandran (%)		
favored	89.0	85.5
allowed	11.0	14.3
generous	0	0.3
disallowed	0	0
root-mean-square deviation		
bond lengths (Å)	0.011	0.005
bond angles (deg)	1.28	0.91

[a]Values in parentheses are for the highest-resolution bin.

RESULTS

Overall Structure of AH. Allophanate hydrolase (AH) was cloned from the genomic DNA of a phylogenetically diverse group of bacteria, including *G. bethesdensis*, *Pseudomonas syringae*, *Wolinella succinogenes*, and *Verminephrobacter eiseniae*. Only *G. bethesdensis* AH (*Gb*AH) was amenable to crystallization. *G. bethesdensis* is an emerging opportunistic pathogen, first isolated in 2006 from patients with chronic granulomatous disease.[29] The X-ray crystal structure of *Gb*AH with malonate was determined by molecular replacement using a putative amidase (PDB entry 2DC0, sequence 32% identical to that of *Gb*AH) as a search model and was refined to 2.2 Å resolution. The apo *Gb*AH structure was determined to 2.8 Å using *Gb*AH with sodium malonate (4GYS) as a search model (Table 1). A large number of overlapping reflections in the data set collected for the apo *Gb*AH structure resulted in acceptable but higher than optimal values for R_{merge}, R, and R_{free}. For this reason, descriptions of the apo *Gb*AH structure are limited to comparative analyses of global and active site structure, and the figures and conclusions presented here are based entirely on the high-quality structure of *Gb*AH with malonate.

In both the apo and ligand-bound structures, the *Gb*AH crystal lattice is composed of a homodimer in the asymmetric unit (Figure 1A). In malonate-bound *Gb*AH, each subunit includes 461 residues (residues 3−463), while in the apo *Gb*AH structure, each subunit includes 462 residues (residues 2−463). In all cases,

dx.doi.org/10.1021/bi301242m | *Biochemistry* 2013, 52, 690−700

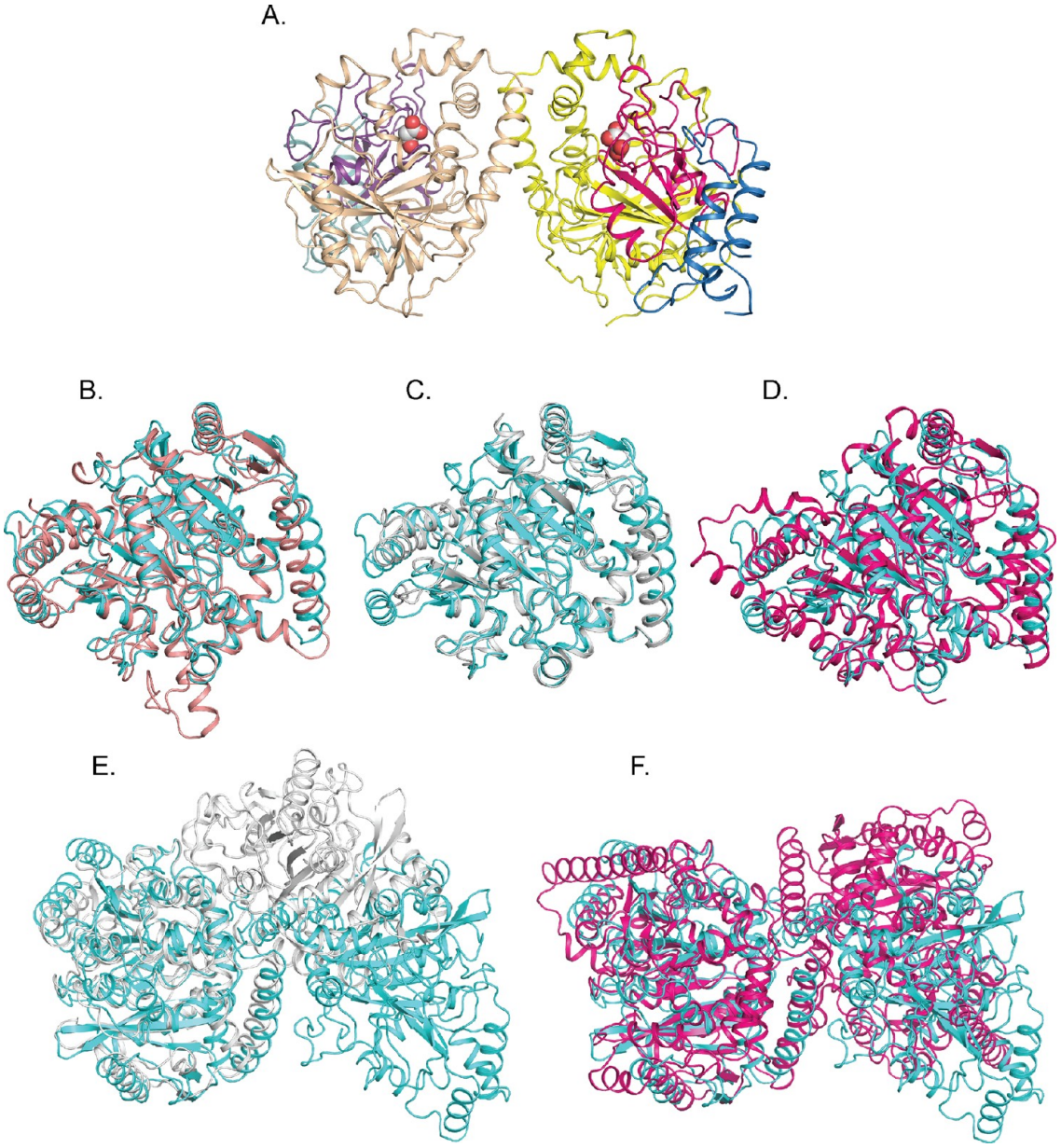

Figure 1. Structure of *Gb*AH and structural comparison with other AS family enzymes. (A) Overall structure of AH. The overall structure is shown as a cartoon. Malonate binding at the active sites is shown in CPK-colored spheres. The three subdomains in each subunit are individually colored: blue for the N-terminal subdomain, hot pink for the amidase signature sequence (Phe_{71}–Leu_{182}) subdomain, and yellow for the C-terminal subdomain. The corresponding subdomains in the second subunit are colored light blue, light pink, and light yellow, respectively. (B–D) Structural superimposition of the *Gb*AH monomer (cyan) with other AS family enzymes. (B) Alignment of AH and *Staphylococcus aureus* GatA (PDB entry 2F2A, salmon). (C) Alignment of AH and *Bradyrhizobium japonicum* malonamidase (MAE2, PDB entry 1OCL) subunit A (white). (D) Alignment of AH and rat fatty acid amide hydrolase (FAAH, PDB entry 1MT5) subunit A (magenta). (E and F) Structural superimposition of the *Gb*AH dimer (cyan) with other AS family enzyme dimers: (E) MAE2 (white) and (F) FAAH (magenta).

the subunits consist of a globular amidase domain comprised of 15 α-helices and 11 β-strands, consistent with structures from other AS family enzymes.[11] The N-terminal poly-His tag and C-terminal residues 463–592 were not defined in the electron density of either the apo or malonate-bound structure and are not included in the models. SDS–PAGE of isolated *Gb*AH crystals grown in the presence of malonate demonstrated that the complete 65 kDa protein was intact in the crystals (data not shown). Therefore, the undefined C-terminus results from a lack of direct phasing information combined with intrinsic disorder in this region. Structural alignments of *Gb*AH with other AS family enzymes show conservation of the overall structure despite low degrees of sequence similarity, ranging from 9 to 32% (Figure 1B–D). Analysis of the AH structure using the DALI server[30] confirms that AH is homologous with several AS family member enzymes (Table S1 of the Supporting Information). Glutamyl-tRNA amidotransferase subunit A (GatA) is the most closely related in structure, as measured by both z score and root-mean-square deviation.

Analytical gel filtration analysis of *Gb*AH revealed a holoenzyme with a molecular mass of ~130 kDa, while SDS–PAGE revealed an ~65 kDa monomer (data not shown), confirming that the biological unit is a dimer, consistent with characterization of other AH enzymes.[15,17] The dimerization

dx.doi.org/10.1021/bi301242m | *Biochemistry* 2013, 52, 690–700

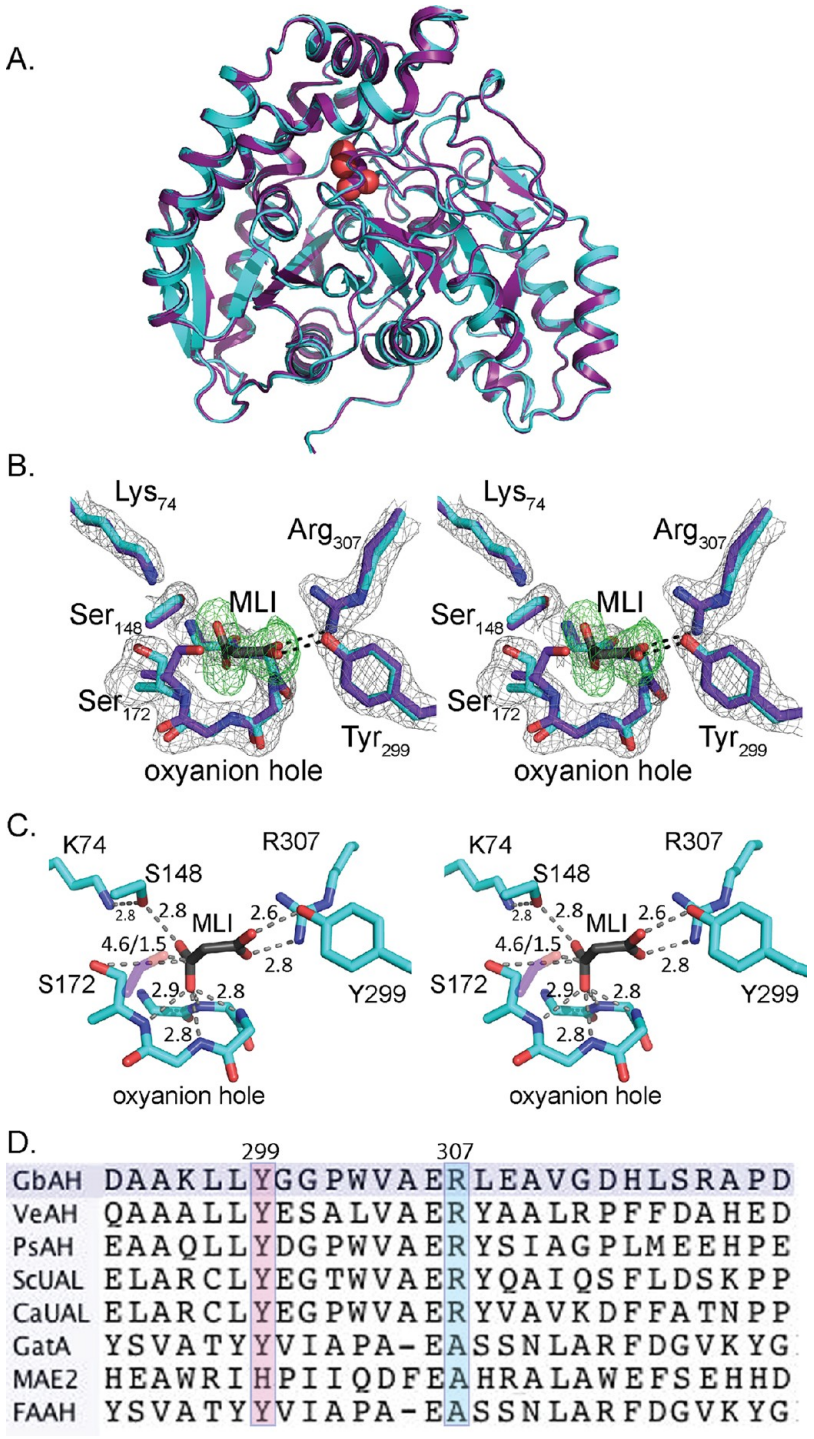

Figure 2. Structural superposition of apo *Gb*AH with the malonate-bound structure. (A) Superimposition of the *Gb*AH monomer with (cyan) and without (purple) bound malonate reveals no significant conformational changes accompanying substrate binding. The active site-bound malonate is shown as CPK-colored spheres. (B) Stereoview showing the structural superimposition of the active sites of apo *Gb*AH (purple) and malonate-bound *Gb*AH (cyan). A simulated annealing omit map for malonate, contoured at 3.0σ, is colored green. The $2F_o - F_c$ map, contoured at 1.0σ, is colored gray. For the sake of clarity, only side chains are displayed for Tyr_{299}, Arg_{307}, Ser_{148}, Ser_{172}, and Lys_{74}. Only main chain atoms are displayed for the oxyanion hole. (C) Stereoview showing the active site of malonate-bound *Gb*AH (cyan). The distances (in angstroms) are indicated. The nucleophilic Ser_{172} adopts a conformation that is oriented away from malonate in the malonate-bound *Gb*AH structure. However, this residue can also adopt an orientation that is oriented toward the substrate's electrophilic center, as observed in the overlaid side chain of Ser_{172} from the apo *Gb*AH structure (transparent purple). (D) Sequence alignment of AH, UAL, and other AS family enzymes shows conservation of Tyr_{299} and Arg_{307} among AH enzymes: *Gb*AH (*G. bethesdensis* allophanate hydrolase), *Ve*AH (*V. eiseniae* allophanate hydrolase), *Ps*AH (*P. syringae* allophanate hydrolase), *Sc*UAL (*Saccharomyces cerevisiae* urea amidolyase), *Ca*UAL (*C. albicans* urea amidolyase), GatA [*Thermotoga maritima* glutamyl-tRNA(Gln) amidotransferase subunit A], MAE2 (*B. japonicum* malonamidase E2), and FAAH (rat fatty acid amide hydrolase).

dx.doi.org/10.1021/bi301242m | *Biochemistry* 2013, 52, 690−700

interface was analyzed using the PDBe PISA server.[31] Three dimerization interfaces were identified as having a large buried surface area and favorable ΔG (Figure S1A of the Supporting Information). The biological dimer was determined to be that with the largest buried surface area and the most favorable ΔG (Figure S1B of the Supporting Information). Of the three possible interfaces, this dimerization interface is most similar, though not identical, to the dimerization interface of the AS family enzymes fatty acid amide hydrolase and malonamidase (Figure 1E,F and Supplementary Figure S1B of the Supporting Information).

***Gb*AH Active Site Architecture.** AH shares a common catalytic mechanism with other AS family members, using a conserved Ser-*cis*-Ser-Lys triad to catalyze amidolysis of allophanate.[17,32] As in other AS family members, three conserved residues, Ser_{172}, *cis*-Ser_{148}, and Lys_{74}, form the expected catalytic triad in *Gb*AH with an oxyanion hole formed by the backbone amide nitrogens of Asp_{168}, Thr_{169}, Ala_{170}, and Gly_{171}. When *Gb*AH was crystallized in sodium malonate (1.04 M), one molecule of malonate was bound at the active site and a second molecule was bound at the protein surface. In crystals grown in the absence of malonate, no electron density corresponding to a bound ligand was observed. The binding of malonate in the active site did not result in any structural rearrangements compared with the ligand-free enzyme (Figure 2A,B). On the basis of the proposed mechanism of homologous AS family enzymes and analysis of inactivated and mutated AH enzymes, Ser_{172} acts as the catalytic nucleophile to attack the amide carbon on allophanate while Ser_{148} acts as a general acid catalyst to stabilize the enzyme−substrate intermediate.[11,17,32] The deprotonated form of Ser_{148} is maintained by Lys_{74} through a hydrogen bond, and the tetrahedral intermediate is stabilized by the oxyanion hole. The catalytic triad facilitates the subsequent hydrolysis of the terminal amide bond to yield a Ser_{172}-dicarboxylated amide and one molecule of NH_3. It is not clear whether the dicarboxylated amide further decomposes while it is tethered to Ser_{172} or is hydrolyzed intact from the enzyme and subsequently decomposes in solution.[32] The nucleophilic Ser_{172} points away from malonate in the bound structure but is oriented toward the active site cavity in the ligand-free enzyme (Figure 2B,C).

The crystal structures of *Gb*AH with bound malonate also reveal two residues, Tyr_{299} and Arg_{307}, within interacting distance (2.6 and 2.8 Å, respectively) of one of the malonate carboxylate moieties (Figure 2C). Sequence alignments reveal that both Tyr_{299} and Arg_{307} are conserved in all AH enzymes but that they are not conserved across the AS family (Figure 2D). This suggests a role for these residues in facilitating substrate binding in the enzyme active site.

The size of the active site cavity is relatively small compared to that of cavities of other AS family enzymes. Measurement of the active site cavity using VOIDOO[33] reveals that the size of the cavity is closest to that of GatA, which uses glutamine or asparagine as a substrate. The cavity size comparison shows a pronounced difference between AH and malonamidase, an AS family enzyme that hydrolyzes a very similar substrate, malonamate.

***Gb*AH Enzyme Activity.** The k_{cat} for wild-type *Gb*AH is 18.2 s^{-1}; the K_m is 0.10 mM, and the k_{cat}/K_m is 1.8×10^5 s^{-1} M^{-1} (Table 2). This falls in a range of k_{cat}/K_m values previously determined for AH from *Oleomonas sagaranensis* (2.7×10^6 s^{-1} M^{-1}),[15] AtzF from *Pseudomonas* sp. strain ADP (1.1×10^4 s^{-1} M^{-1}),[17] and TrzF from *Enterobacter cloacae* strain 99 (8.8×10^3 s^{-1} M^{-1}).[32]

Table 2. Kinetic Data of Wild-Type *Gb*AH and Its Site-Directed Mutants with Allophanate

	k_{cat} (s^{-1})[a]	K_m (mM)[a]	k_{cat}/K_m[b] (s^{-1} M^{-1})
wild type	18 ± 1	0.10 ± 0.002	$(1.8 \pm 0.03) \times 10^5$
C_del	20 ± 1	0.30 ± 0.004	$(6.9 \pm 0.2) \times 10^4$
Y299F	$(4.2 \pm 0.1) \times 10^{-2}$	1.2 ± 0.1	35 ± 3
Y299A	$(7.1 \pm 0.2) \times 10^{-2}$	3.0 ± 0.4	24 ± 3
R307A	–	–	$(1.7 \pm 0.2) \times 10^{-3}$
R307M	–	–	$(3.6 \pm 0.8) \times 10^{-3}$
Y299A/R307M	–	–	$(1.9 \pm 0.1) \times 10^{-2}$
Y299F/R307M	–	–	$(7.1 \pm 0.6) \times 10^{-3}$
Y299A/R307A	–	–	$(2.7 \pm 0.2) \times 10^{-2}$

[a]Mean ± standard deviation (n = 3). [b]k_{cat}/K_m estimated from the slope of v_i vs [S] at [S] ≪ K_m; mean ± standard deviation (n = 3).

Substrate Specificity. AH has been shown to exhibit high specificity for allophanate.[15,32] To assess the substrate specificity of *Gb*AH, the rate of ammonia release was measured for a series of allophanate analogues, including biuret, malonamide, acetylurea, hydantoic acid, L-glutamine, and L-asparagine (Figure S2 of the Supporting Information). Among this group of substrate analogues, activity was only detected with biuret and malonamide, consistent with previous reports.[32] The measured kinetic constants for *Gb*AH with allophanate and the substrate analogues biuret and malonamide are listed in Table 3 with representative data provided in Figure S3 of the Supporting Information.

Tyr_{299} and Arg_{307} are within hydrogen bonding distance (2.6 and 2.8 Å, respectively) of one carboxylate moiety of malonate (Figure 2C). Both Tyr_{299} and Arg_{307} were mutated in *Gb*AH to investigate the role of these two residues in catalysis. A series of single mutants (Y299F, Y299A, R307M, and R307A) and double mutants (Y299A/R307M, Y299F/R307M, Y299A/R307A, and Y299F/R307A) were assayed for catalytic activity. While the dimerization interface is located in the proximity of the active sites, analytical gel filtration confirmed that mutations in the active site residues located near the interface (i.e., Ser_{172}, Tyr_{299}, and Arg_{307}) did not alter the oligomerization state of the enzyme (Figure S4 of the Supporting Information). The kinetic constants measured with allophanate revealed ∼400- and ∼250-fold reductions in k_{cat} for Y299F and Y299A, respectively, and ∼5000- and ∼7500-fold reductions in k_{cat}/K_m for Y299F and Y299A, respectively (Table 2). In addition, mutations of Tyr_{299} altered the enzyme's discrimination between substrates, increasing the specificity constants for biuret and malonamide relative to that for allophanate. The k_{cat}/K_m ratio for biuret compared to that for allophanate increased by 3 orders of magnitude in Y299F and 4 orders of magnitude in Y299A (Table 3). By comparison, mutations of Arg_{307} had a much more dramatic effect on the rate of catalysis. The k_{cat}/K_m is estimated to be $2-4 \times 10^{-3}$ s^{-1} M^{-1} for Arg_{307} mutants, resulting in a decrease in k_{cat}/K_m of 8 orders of magnitude. No activity could be observed for Arg_{307} mutants with biuret or malonamide.

Function of the C-Terminal Domain. While the structures in the presence and absence of malonate defined the 462-amino acid globular amidase domain, the 126 C-terminal amino acids were disordered in both structures. This suggests that an additional, less structured domain of unknown function resides at

Table 3. Kinetic Data for Wild-Type *Gb*AH and Its Mutants with Substrate Analogues

	biuret k_{cat}/K_m[a] (s^{-1} M^{-1})	$[k_{cat}/K_m$(biuret)]/ $[k_{cat}/K_m$(allophanate)]	ratio to wild type	malonamide k_{cat}/K_m[a] (s^{-1} M^{-1})	$[k_{cat}/K_m$(malonamide)]/ $[k_{cat}/K_m$(allophanate)]	ratio to wt
wild type	0.30 ± 0.01	$(1.7 \pm 0.1) \times 10^{-6}$	1	0.38 ± 0.01	$(2.1 \pm 0.2) \times 10^{-6}$	1
C_del	0.59 ± 0.02	$(8.6 \pm 0.4) \times 10^{-6}$	5.2	0.35 ± 0.01	$(5.1 \pm 0.2) \times 10^{-6}$	2.4
Y299F	0.35 ± 0.02	$(1.0 \pm 0.1) \times 10^{-2}$	6.1×10^3	0.12 ± 0.01	$(3.5 \pm 0.1) \times 10^{-3}$	1.6×10^3
Y299A	1.0 ± 0.02	$(4.3 \pm 0.6) \times 10^{-2}$	2.6×10^4	0.36 ± 0.02	$(1.5 \pm 0.2) \times 10^{-2}$	7.2×10^3

[a] k_{cat}/K_m estimated from the slope of v_i vs [S] at [S] $\ll K_m$; mean ± standard deviation (n = 3).

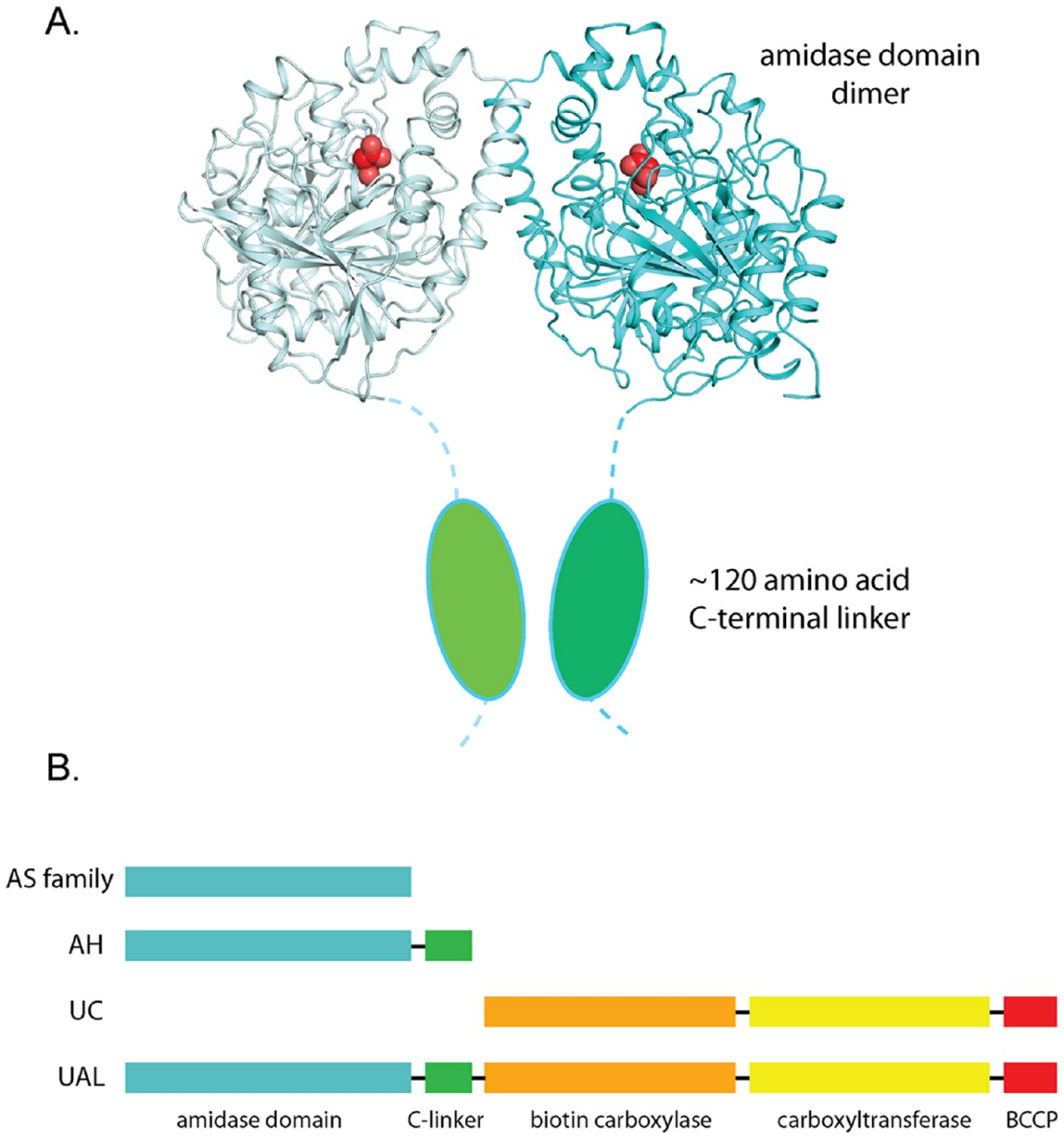

Figure 3. C-Terminal domain of *Gb*AH. (A) Structure of the amidase domain of AH with a cartoon representation showing the missing C-terminal domain, depicted as green ovals encircled by a dotted line. (B) Schematic representation of the domain arrangement of AH, urea carboxylase, urea amidolyase, and other AS family enzymes.

the C-terminus of AH. This domain is conserved in all AH enzymes but is missing in other AS family enzymes (Figure 3). To determine whether the C-terminal domain influences the overall amidase activity, the 126 C-terminal amino acids were truncated by introducing two stop codons immediately following the codon encoding the last ordered residue from the crystal structure, Thr_{462}. The C-terminally truncated enzyme was overexpressed and purified, and the molecular mass was confirmed to be ~50 kDa by SDS−PAGE, compared to the full-length ~65 kDa wild-type enzyme. The truncated enzyme maintained its ability to dimerize, as measured by analytical gel filtration (Figure S4 of the Supporting Information). Further-

more, truncation of the C-terminus had very little effect on the kinetic constants. The k_{cat} and K_m values measured for the C-terminal truncation were very similar to those measured for the wild-type enzyme, both with the substrate and with substrate analogues (Tables 2 and 3), indicating that the C-terminal domain does not significantly influence amidase activity or substrate specificity.

DISCUSSION

Acylamide amidohydrolase enzymes (EC classification group 3.5.1) catalyze the hydrolysis of linear amide bonds in a wide range of substrates. Several enzyme superfamilies with unrelated sequence and structure have converged on this common enzymatic function, including the amidohydrolase, nitrilase, and amidase signature (AS) superfamilies. Members of the AS superfamily catalyze amidolysis without the assistance of a metal ion, instead using a nucleophilic serine and oxyanion hole to mediate the formation and stabilization of the tetrahedral transition state. The superfamily was originally identified and characterized by a signature block of 130 amino acids rich in conserved Gly and Ser residues.[2] Subsequent structural and kinetic studies of AS family enzymes revealed a conserved Ser-*cis*-Ser-Lys catalytic triad that is essential for catalysis.[11,34−36] The structures of a few well-characterized members of the AS family have been reported in recent years, including those of GatA,[37] malonamidase,[11] fatty acid amide hydrolase,[38] and peptide amidase.[39] These structures have confirmed a common catalytic core and have revealed a diverse active site architecture that accommodates both stringent and promiscuous activities over a wide range of substrates.

AH is a typical AS family enzyme using a Ser-*cis*-Ser-Lys catalytic triad to hydrolyze allophanate to ammonia and carbon dioxide. In some bacterial strains, AH works in conjunction with cyanuric acid amidohyrolase (EC 3.5.2.15) and biuret amidohydrolase (EC 3.5.1.84) to catalyze the final steps of *s*-triazide degradation.[17,32,40] In certain fungi and prokaryotes, AH functions in concert with urea carboxylase to degrade urea.[16,41] Prior to this investigation, no structure of AH had been reported. Several studies have described a high degree of substrate specificity in AH,[15,17,32] but in the absence of structural insights, the molecular basis for this specificity has not been defined.

General Features of the AH Structure. Both the overall fold and the position of the catalytic triad in *Gb*AH superimpose well with those of other members of the AS family. However, comparison of the AH dimer with homologous structures reveals that the superfamily exhibits a surprising plasticity at the dimerization interface. A structural alignment of *Gb*AH with dimeric superfamily members shows that the dimerization interface varies between enzymes, leading to a wide variation in the distance between active sites, ranging from 33 to 60 Å (Figure 1E,F). The absence of a conserved dimerization interface in the AS family suggests that dimerization does not play an essential role in catalysis and that the individual active sites most likely function independently. Indeed, some AS family members do not form homodimers: GatA, the glutamine amidohydrolase component of GatCAB, makes up a heterotrimer with GatB and GatC subunits,[5] and in vivo and in vitro studies of *Arabidopsis* amidase-1 have concluded that there is no interaction between the amidase monomers.[42] Nevertheless, the relationship between dimerization and catalytic activity in AH warrants further investigation considering that the essential active site residues Tyr_{299} and Arg_{307} (vide infra) are positioned near the dimerization interface. A connection between dimerization and substrate specificity has been proposed for the AS family nitrile amidase from *Rhodococcus* sp. N-771, in which a modified dimerization interface reduces the width of the substrate binding tunnel, thereby limiting the access of larger substrates.[6]

Comparison of the ligand-free and malonate-bound structures of *Gb*AH reveals no structural rearrangements accompanying ligand binding in the active site (Figure 2B), consistent with other AS family enzymes.[8,11] Thus, from X-ray structures, it appears that the active sites of AS enzymes are rigid assemblies and that substrate discrimination arises by limiting substrate access to the active site and by the design of specific architectures that are complementary to the substrate(s). This apparent rigidity of AS active sites makes the superfamily particularly amenable to functional predictions by in silico ligand docking, as described in a recent review.[43]

Substrate Specificity Determinants in AH. Previous studies of AH cloned from *E. cloacae* (TrzF) and *Pseudomonas* sp. strain ADP (AtzF) confirmed the identity of the Ser-*cis*-Ser-Lys catalytic triad and documented a detectable promiscuous activity with the alternate substrates biuret, malonamide, and malonamate.[17,32] TrzF has a specific activity of 0.5 nmol min^{-1} mg^{-1} with biuret and 1.5 nmol min^{-1} mg^{-1} with malonamide.[32] *Gb*AH has a similar activity of 8.3 nmol min^{-1} mg^{-1} with biuret and 2.3 nmol min^{-1} mg^{-1} with malonamide. Conversely, AH from *Oleomonas sagaranensis* had no detectable activity with biuret or malonamide.[15] Whereas the identity of the catalytic triad and the low tolerance for analogous substrates have been documented in AH, the active site residues contributing to substrate recognition have not been described because of a lack of structural information. In this study, the structure of the *Gb*AH−malonate complex combined with kinetic analysis of *Gb*AH modified by site-directed mutagenesis has revealed an important role for two conserved residues, Tyr_{299} and Arg_{307}. The side chains for these amino acids are positioned 2.6−2.8 Å from the carboxylate moiety of the substrate analogue, malonate (Figure 2C). Mutations of Arg_{307} result in a nearly complete loss of catalytic activity, while mutations of Tyr_{299} substantially decrease k_{cat} and k_{cat}/K_m for allophanate and reduce the substrate preference of AH for allophanate compared with those for biuret and malonamide (Tables 2 and 3).

While malonate is not an ideal isosteric mimic of allophanate, the *Gb*AH structure with bound malonate can be combined with kinetic analysis of *Gb*AH site-directed mutations to propose a role for Tyr_{299} and Arg_{307} in AH catalysis. The side chain of Tyr_{299} is 2.6 Å from the carboxylate oxygen of malonate. This residue is proposed to donate a hydrogen bond to the deprotonated carboxylate of allophanate. The donation of a hydrogen bond from Tyr_{299} would facilitate discrimination between the carboxylate moiety of the bona fide substrate, allophanate, and the amide substituent of the substrate analogues, biuret and malonamide. The reduced level of discrimination between allophanate and malonamide/biuret in Tyr_{299} mutations is consistent with this proposal. In addition, the side chain of Arg_{307} is 2.8 Å from the other carboxylate oxygen of malonate, suggesting that Arg_{307} interacts with the substrate carboxylate via a salt bridge in a manner analogous to interactions with substrate carboxylate moieties in malonamidase and GatA (vide infra). The nearly complete loss of catalytic activity with allophanate observed in site-directed mutations at Arg_{307} is consistent with this proposal. The formation of a salt bridge between Arg_{307} and the substrate would serve to bind and orient the substrate in the proximity of the catalytic triad and also to assist in stabilizing developing negative charge in the transition state. The inability of

dx.doi.org/10.1021/bi301242m | *Biochemistry* 2013, 52, 690−700

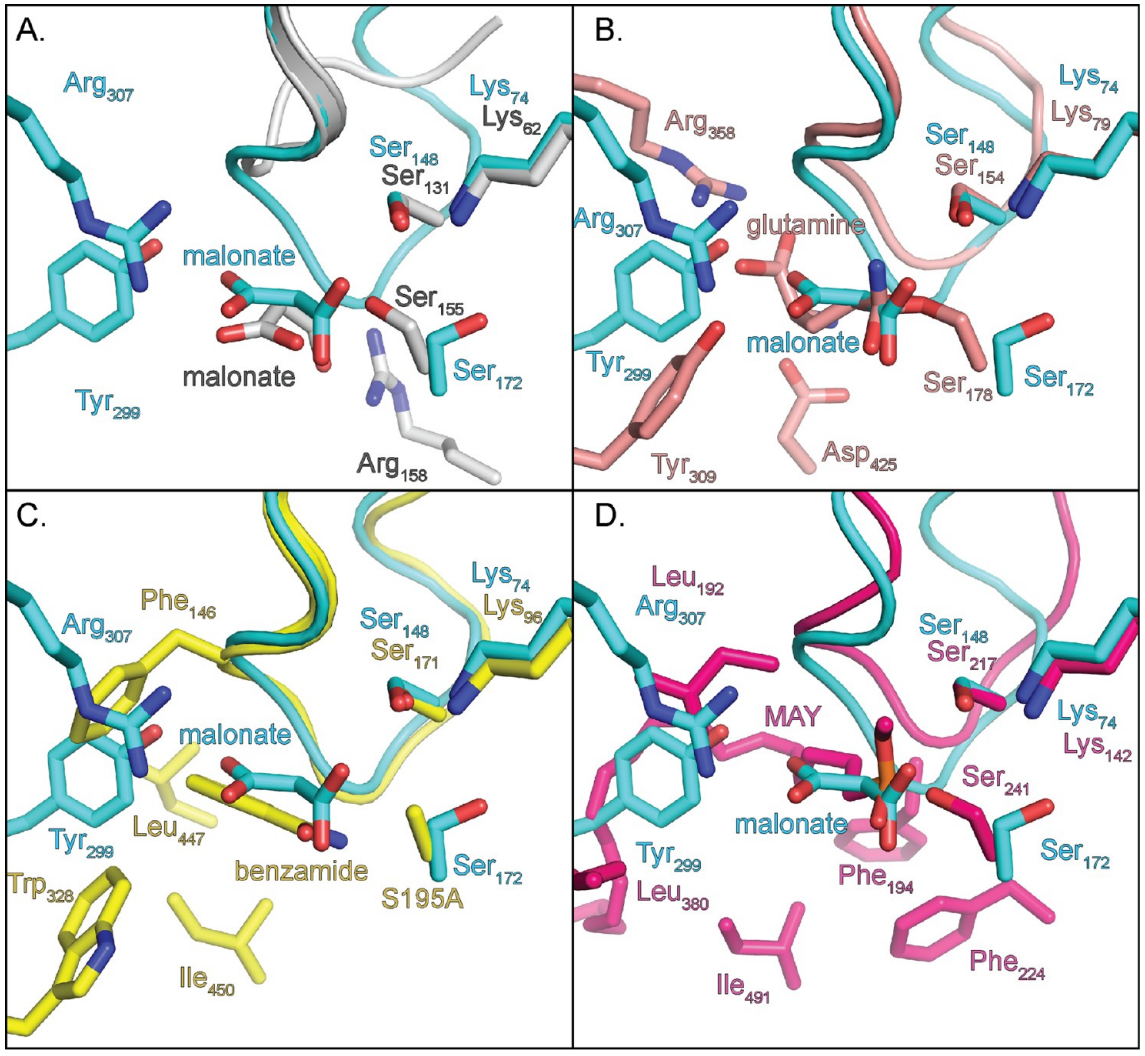

Figure 4. Comparison of substrate binding residues at the active sites of *Gb*AH with other AS family enzymes. (A) Alignment of malonate-bound *Gb*AH (cyan) and malonate-bound *B. japonicum* malonamidase (PDB entry 1OCL, white). (B) Alignment of malonate-bound *Gb*AH (cyan) and *S. aureus* GatA with covalently bound glutamine (PDB entry 2F2A, salmon). (C) Alignment of malonate-bound *Gb*AH (cyan) and benzamide-bound *Rhodococcus* sp. N-771 amidase (PDB entry 3A1I, yellow). (D) Alignment of malonate-bound *Gb*AH (cyan) with rat fatty acid amide hydrolase (PDB entry 1MT5, pink) with the bound inactivator methoxy arachidonyl fluorophosphonate (MAY). Residues and substrates are shown as sticks, labeled and colored according to their structure.

wild-type AH to form a salt bridge with the alternate substrates biuret and malonamide may further account for the poor reactivity of these substrates. Substrate discrimination in AH, therefore, may originate from anchoring the carboxylate moiety of allophanate in the active site opposite the catalytic triad and, thus, properly positioning and orienting the amide portion of the substrate for nucleophilic attack. It is conceivable that substrate analogues such as biuret, malonamide, and asparagine are anchored improperly and, consequently, the terminal amide of these substrates is improperly positioned for attack by the Ser_{172} nucleophile of the catalytic triad. Confirmation of this proposal awaits structures of *Gb*AH bound with alternate substrates.

Malonamate is a structural analogue of allophanate and the substrate of the AS family enzyme, malonamidase. Given the similarity between the substrates, these two enzymes might be expected to share similar active site architectures. However, structural and phylogenetic analysis[17] reveals that malonamidase and AH are distantly related AS superfamily members. Instead, AH is most closely related to GatA, bacterial glutamyl-tRNA amidotransferase subunit A. Interestingly, all three of these enzymes position an Arg side chain for salt bridge formation with the substrate carboxylate moiety while AS family enzymes acting on non-carboxylated substrates do not (Figure 4). In malonamidase, this residue (Arg_{158}) is located on the opposite side of the active site compared with its location in AH and GatA, resulting in a completely different substrate binding orientation (Figure 3A). This arginine is replaced by a valine in AH and a glutamine in GatA. In addition, an active site loop (amino acids 119−125 in *Gb*AH) present in most AS family enzymes adopts a variety of conformations and contributes to substrate specificity by dictating the orientation of the substrate in the active site. In malonamidase, this loop adopts an atypical conformation, forcing the substrate into a different binding orientation (Figure 4A and Figure S5 of the Supporting Information).

The substrate binding orientation and the position and identity of the side chains responsible for substrate binding are very similar between GatA and AH (Figure 4B). In the GatA structure, an alanine replaces Arg_{307} of *Gb*AH. However, GatA positions a different arginine side chain at a similar location in the active site, allowing the guanidinium side chain to form a salt

dx.doi.org/10.1021/bi301242m | *Biochemistry* 2013, 52, 690−700

bridge with the substrate carboxylate. This guanidinium group is 7 Å further removed from the catalytic triad in GatA than in *Gb*AH, allowing the longer substrates, asparagine and glutamine, to be properly positioned in the triad of GatA. It is notable that AH does not catalyze the hydrolysis of either glutamine or asparagine. The difference in the arginine side chain position may explain this discrimination, accounting for the specificity of GatA for longer substrates and AH for shorter substrates. In the heterotrimeric GatCAB complex, an ammonia channel runs from the GatA glutaminase active site to the transamidase catalytic pocket in GatB.[5,37] This same channel appears to be present in *Gb*AH and may serve as an exit channel for the release of the ammonia (Figure S6 of the Supporting Information).

A Structurally Independent C-Terminal Domain in AH. The structures of *Gb*AH reveal the presence of a unique C-terminal domain that is not present in other AS family enzymes but is conserved in AH and urea amidolyase. Deletion of this domain did not significantly influence the dimerization or catalytic activity of *Gb*AH. The functional role of this domain, therefore, cannot yet be unambiguously assigned. However, given that AH activity is typically coupled to the reaction of urea carboxylase and that they comprise separate domains of urea amidolyase in yeast (Figure 3B), it is tempting to speculate that the C-terminal domain of AH facilitates the interaction and coupling between AH and urea carboxylase enzymes or between the individual catalytic domains in urea amidolyase. In the heterotrimeric GatCAB, a small GatC subunit links GatA and GatB and is essential for maintaining GatCAB structure and activity.[37,44,45] In bacteria, the genes encoding urea carboxylase and AH are tightly clustered, suggesting that they may coordinate their activities.[16] However, studies examining the interaction between urea carboxylase and AH indicate that AH and urea carboxylase do not form a stable complex,[15] consistent with studies of AH and urea carboxylase from *P. syringae* (Figure S7 of the Supporting Information). The absence of a stable complex between AH and urea carboxylase does not, however, preclude the possibility of a transient interaction between the two enzymes that may serve to facilitate the efficient transfer of intermediates.[46,47] Furthermore, additional proteins may be required to maintain a stable complex between AH and urea carboxylase. It is notable that two additional putative cytoplasmic proteins of unknown function (GenBank entries YP_745567 and YP_745568 in *G. bethesdensis*) are located in the proximity of the genes for AH and urea carboxylase in many bacteria. Structural and kinetic studies are currently underway to clarify whether additional proteins mediate multienzyme complex formation via the C-terminal domain of AH and to determine the extent of substrate channeling that exists between urea carboxylase and AH.

■ ASSOCIATED CONTENT

Supporting Information

Supplementary methods, Table S1, and Figures S1–S7. This material is available free of charge via the Internet at http://pubs.acs.org.

Accession Codes

The atomic coordinates for apo *Gb*AH and *Gb*AH with malonate have been deposited as Protein Data Bank entries 4GYR and 4GYS, respectively.

■ AUTHOR INFORMATION

Corresponding Author

*Department of Biological Sciences, Marquette University, P.O. Box 1881, Milwaukee, WI 53201. Phone: (414) 288-2087. Fax: (414) 288-7357. E-mail: martin.stmaurice@marquette.edu.

Funding

This work is supported by National Institute of General Medical Sciences Grant R15GM097724.

Notes

The authors declare no competing financial interest.

■ ACKNOWLEDGMENTS

Use of the Advanced Photon Source was supported by the U.S. Department of Energy, Office of Science, Office of Basic Energy Sciences, under Contract DE-AC02-06CH11357. Use of LS-CAT Sector 21 was supported by the Michigan Economic Development Corp. and the Michigan Technology Tri-Corridor for the support of this research program (Grant 085P1000817).

■ ABBREVIATIONS

AH, allophanate hydrolase; APS, Advanced Photon Source; AS, amidase signature; DTT, dithiothreitol; EGTA, ethylene glycol bis(2-aminoethyl ether)-*N*,*N*,*N*′,*N*′-tetraacetic acid; GatA, glutamyl-tRNA amidotransferase subunit A; GatCAB, heterotrimeric glutamyl-tRNA amidotransferase CAB; *Gb*AH, *G. bethesdensis* allophanate hydrolase; GDH, glutamate-dehydrogenase; Gln-tRNA^{Gln}, glutaminyl-tRNA^{Gln}; HEPES, 4-(2-hydroxyethyl)-1-piperazineethanesulfonic acid; IPTG, isopropyl β-D-1-thiogalactopyranoside; NADH, reduced nicotinamide adenine dinucleotide; TEV, tobacco etch virus; PEG, poly(ethylene glycol); PIPES, piperazine-*N*,*N*′-bis(2-ethanesulfonic acid); SDS–PAGE, sodium dodecyl sulfate–polyacrylamide gel electrophoresis.

■ REFERENCES

(1) Koo, H. M., Choi, S. O., Kim, H. M., and Kim, Y. S. (2000) Identification of Active-Site Residues in *Bradyrhizobium japonicum* Malonamidase E2. *Biochem. J. 349*, 501–507.

(2) Chebrou, H., Bigey, F., Arnaud, A., and Galzy, P. (1996) Study of the Amidase Signature Group. *Biochim. Biophys. Acta 1298*, 285–293.

(3) Shin, S., Yun, Y. S., Koo, H. M., Kim, Y. S., Choi, K. Y., and Oh, B. H. (2003) Characterization of a Novel Ser-cisSer-Lys Catalytic Triad in Comparison with the Classical Ser-His-Asp Triad. *J. Biol. Chem. 278*, 24937–24943.

(4) Boger, D. L., Fecik, R. A., Patterson, J. E., Miyauchi, H., Patricelli, M. P., and Cravatt, B. F. (2000) Fatty Acid Amide Hydrolase Substrate Specificity. *Bioorg. Med. Chem. Lett. 10*, 2613–2616.

(5) Wu, J., Bu, W., Sheppard, K., Kitabatake, M., Kwon, S. T., Soll, D., and Smith, J. L. (2009) Insights into tRNA-Dependent Amidotransferase Evolution and Catalysis from the Structure of the *Aquifex aeolicus* Enzyme. *J. Mol. Biol. 391*, 703–716.

(6) Ohtaki, A., Murata, K., Sato, Y., Noguchi, K., Miyatake, H., Dohmae, N., Yamada, K., Yohda, M., and Odaka, M. (2010) Structure and Characterization of Amidase from *Rhodococcus* sp. N-771: Insight into the Molecular Mechanism of Substrate Recognition. *Biochim. Biophys. Acta 1804*, 184–192.

(7) Kim, Y. S., and Kang, S. W. (1994) Novel Malonamidases in *Bradyrhizobium japonicum*. Purification, Characterization, and Immunological Comparison. *J. Biol. Chem. 269*, 8014–8021.

(8) Yasuhira, K., Shibata, N., Mongami, G., Uedo, Y., Atsumi, Y., Kawashima, Y., Hibino, A., Tanaka, Y., Lee, Y. H., Kato, D., Takeo, M., Higuchi, Y., and Negoro, S. (2010) X-ray Crystallographic Analysis of the 6-Aminohexanoate Cyclic Dimer Hydrolase: Catalytic Mechanism

and Evolution of an Enzyme Responsible for Nylon-6 Byproduct Degradation. *J. Biol. Chem. 285*, 1239−1248.
(9) Heumann, S., Eberl, A., Fischer-Colbrie, G., Pobeheim, H., Kaufmann, F., Ribitsch, D., Cavaco-Paulo, A., and Guebitz, G. M. (2009) A Novel Aryl Acylamidase from *Nocardia farcinica* Hydrolyses Polyamide. *Biotechnol. Bioeng. 102*, 1003−1011.
(10) Cerovsky, V., and Kula, M. R. (2001) Studies on Peptide Amidase-Catalysed C-Terminal Peptide Amidation in Organic Media with Respect to its Substrate Specificity. *Biotechnol. Appl. Biochem. 33*, 183−187.
(11) Shin, S., Lee, T. H., Ha, N. C., Koo, H. M., Kim, S. Y., Lee, H. S., Kim, Y. S., and Oh, B. H. (2002) Structure of Malonamidase E2 Reveals a Novel Ser-*cis*Ser-Lys Catalytic Triad in a New Serine Hydrolase Fold that is Prevalent in Nature. *EMBO J. 21*, 2509−2516.
(12) Roon, R. J., Hampshire, J., and Levenberg, B. (1972) Urea Amidolyase. The Involvement of Biotin in Urea Cleavage. *J. Biol. Chem. 247*, 7539−7545.
(13) Ghosh, S., Navarathna, D. H., Roberts, D. D., Cooper, J. T., Atkin, A. L., Petro, T. M., and Nickerson, K. W. (2009) Arginine-Induced Germ Tube Formation in *Candida albicans* is Essential for Escape from Murine Macrophage Line RAW 264.7. *Infect. Immun. 77*, 1596−1605.
(14) Fan, C., Chou, C. Y., Tong, L., and Xiang, S. (2012) Crystal Structure of Urea Carboxylase Provides Insights into the Carboxyltransfer Reaction. *J. Biol. Chem. 287*, 9389−9398.
(15) Kanamori, T., Kanou, N., Kusakabe, S., Atomi, H., and Imanaka, T. (2005) Allophanate Hydrolase of *Oleomonas sagaranensis* Involved in an ATP-Dependent Degradation Pathway Specific to Urea. *FEMS Microbiol. Lett. 245*, 61−65.
(16) Strope, P. K., Nickerson, K. W., Harris, S. D., and Moriyama, E. N. (2011) Molecular Evolution of Urea Amidolyase and Urea Carboxylase in Fungi. *BMC Evol. Biol. 11*, 80.
(17) Shapir, N., Sadowsky, M. J., and Wackett, L. P. (2005) Purification and Characterization of Allophanate Hydrolase (AtzF) from *Pseudomonas* sp. Strain ADP. *J. Bacteriol. 187*, 3731−3738.
(18) Cheng, G., Shapir, N., Sadowsky, M. J., and Wackett, L. P. (2005) Allophanate Hydrolase, Not Urease, Functions in Bacterial Cyanuric Acid Metabolism. *Appl. Environ. Microbiol. 71*, 4437−4445.
(19) Whitney, P. A., and Cooper, T. G. (1972) Urea Carboxylase and Allophanate Hydrolase. Two Components of Adenosine Triphosphate:Urea Amido-Lyase in *Saccharomyces cerevisiae*. *J. Biol. Chem. 247*, 1349−1353.
(20) Lietzan, A. D., Menefee, A. L., Zeczycki, T. N., Kumar, S., Attwood, P. V., Wallace, J. C., Cleland, W. W., and St Maurice, M. (2011) Interaction between the Biotin Carboxyl Carrier Domain and the Biotin Carboxylase Domain in Pyruvate Carboxylase from *Rhizobium etli*. *Biochemistry 50*, 9708−9723.
(21) Gasteiger, E., Gattiker, A., Hoogland, C., Ivanyi, I., Appel, R. D., and Bairoch, A. (2003) ExPASy: The Proteomics Server for in-Depth Protein Knowledge and Analysis. *Nucleic Acids Res. 31*, 3784−3788.
(22) Otwinowski, Z., and Minor, W. (1997) Processing of X-ray Diffraction Data Collected in Oscillation Mode. *Methods Enzymol. 276*, 307−326.
(23) McCoy, A. J., Grosse-Kunstleve, R. W., Adams, P. D., Winn, M. D., Storoni, L. C., and Read, R. J. (2007) Phaser Crystallographic Software. *J. Appl. Crystallogr. 40*, 658−674.
(24) Terwilliger, T. C., Grosse-Kunstleve, R. W., Afonine, P. V., Moriarty, N. W., Zwart, P. H., Hung, L. W., Read, R. J., and Adams, P. D. (2008) Iterative Model Building, Structure Refinement and Density Modification with the PHENIX AutoBuild Wizard. *Acta Crystallogr. D64*, 61−69.
(25) Emsley, P., and Cowtan, K. (2004) Coot: Model-Building Tools for Molecular Graphics. *Acta Crystallogr. D60*, 2126−2132.
(26) Afonine, P. V., Grosse-Kunstleve, R. W., and Adams, P. D. (2005) The Phenix Refinement Framework. *Collaborative Computational Project Number 4 Newsletter*, July.
(27) Kimura, S., Yamanishi, H., Iyama, S., Yamaguchi, Y., and Kanakura, Y. (2003) Enzymatic Assay for Determination of Bicarbonate Ion in Plasma using Urea Amidolyase. *Clin. Chim. Acta 328*, 179−184.
(28) Weatherburn., M. W. (1967) Phenol-Hypochloride Reaction for Determination of Ammonia. *Anal. Chem. 39*, 971−974.
(29) Greenberg, D. E., Porcella, S. F., Stock, F., Wong, A., Conville, P. S., Murray, P. R., Holland, S. M., and Zelazny, A. M. (2006) *Granulibacter bethesdensis* Gen. Nov., Sp. Nov., a Distinctive Pathogenic Acetic Acid Bacterium in the Family Acetobacteraceae. *Int. J. Syst. Evol. Microbiol. 56*, 2609−2616.
(30) Holm, L., and Rosenstrom, P. (2010) Dali Server: Conservation Mapping in 3D. *Nucleic Acids Res. 38*, W545−W549.
(31) Krissinel, E., and Henrick, K. (2007) Inference of Macromolecular Assemblies from Crystalline State. *J. Mol. Biol. 372*, 774−797.
(32) Shapir, N., Cheng, G., Sadowsky, M. J., and Wackett, L. P. (2006) Purification and Characterization of TrzF: Biuret Hydrolysis by Allophanate Hydrolase Supports Growth. *Appl. Environ. Microbiol. 72*, 2491−2495.
(33) Kleywegt, G. J., and Jones, T. A. (1994) Detection, Delineation, Measurement and Display of Cavities in Macromolecular Structures. *Acta Crystallogr. D50*, 178−185.
(34) Valina, A. L., Mazumder-Shivakumar, D., and Bruice, T. C. (2004) Probing the Ser-Ser-Lys Catalytic Triad Mechanism of Peptide Amidase: Computational Studies of the Ground State, Transition State, and Intermediate. *Biochemistry 43*, 15657−15672.
(35) McKinney, M. K., and Cravatt, B. F. (2003) Evidence for Distinct Roles in Catalysis for Residues of the Serine-Serine-Lysine Catalytic Triad of Fatty Acid Amide Hydrolase. *J. Biol. Chem. 278*, 37393−37399.
(36) Shin, S., Lee, T. H., Koo, H. M., Kim, S. Y., Lee, H. S., Kim, Y. S., and Oh, B. H. (2002) Crystallization and Preliminary X-ray Crystallographic Analysis of Malonamidase E2, an Amidase Signature Family Member. *Acta Crystallogr. D58*, 562−563.
(37) Nakamura, A., Yao, M., Chimnaronk, S., Sakai, N., and Tanaka, I. (2006) Ammonia Channel Couples Glutaminase with Transamidase Reactions in GatCAB. *Science 312*, 1954−1958.
(38) Bracey, M. H., Hanson, M. A., Masuda, K. R., Stevens, R. C., and Cravatt, B. F. (2002) Structural Adaptations in a Membrane Enzyme that Terminates Endocannabinoid Signaling. *Science 298*, 1793−1796.
(39) Labahn, J., Neumann, S., Buldt, G., Kula, M. R., and Granzin, J. (2002) An Alternative Mechanism for Amidase Signature Enzymes. *J. Mol. Biol. 322*, 1053−1064.
(40) Garcia-Gonzalez, V., Govantes, F., Porrua, O., and Santero, E. (2005) Regulation of the *Pseudomonas* sp. Strain ADP Cyanuric Acid Degradation Operon. *J. Bacteriol. 187*, 155−167.
(41) Lombard, J., and Moreira, D. (2011) Early Evolution of the Biotin-Dependent Carboxylase Family. *BMC Evol. Biol. 11*, 232.
(42) Pollmann, S., Neu, D., and Weiler, E. W. (2003) Molecular Cloning and Characterization of an Amidase from *Arabidopsis thaliana* Capable of Converting Indole-3-Acetamide into the Plant Growth Hormone, Indole-3-Acetic Acid. *Phytochemistry 62*, 293−300.
(43) Gerlt, J. A., Babbitt, P. C., Jacobson, M. P., and Almo, S. C. (2012) Divergent Evolution in Enolase Superfamily: Strategies for Assigning Functions. *J. Biol. Chem. 287*, 29−34.
(44) Nagao, A., Suzuki, T., Katoh, T., Sakaguchi, Y., and Suzuki, T. (2009) Biogenesis of Glutaminyl-Mt $tRNA^{Gln}$ in Human Mitochondria. *Proc. Natl. Acad. Sci. U.S.A. 106*, 16209−16214.
(45) Sheppard, K., and Soll, D. (2008) On the Evolution of the tRNA-Dependent Amidotransferases, GatCAB and GatDE. *J. Mol. Biol. 377*, 831−844.
(46) Geck, M. K., and Kirsch, J. F. (1999) A Novel, Definitive Test for Substrate Channeling Illustrated with the Aspartate Aminotransferase/Malate Dehydrogenase System. *Biochemistry 38*, 8032−8037.
(47) James, C. L., and Viola, R. E. (2002) Production and Characterization of Bifunctional Enzymes. Substrate Channeling in the Aspartate Pathway. *Biochemistry 41*, 3726−3731.